Control concepts of a radiant wall working as thermal energy storage for peak load shifting of a heat pump coupled to a PV array

Joaquim Romaní[1], Martin Belusko[2], Alemu Alemu[2], Luisa F. Cabeza[1], Alvaro de Gracia[3,*], Frank Bruno[2]

[1]GREA Innovació concurrent, INSPIRES Research Centre, University of Lleida, Pere de Cabrera s/n, 25001, Lleida, Spain

[2]Barbara Hardy Institute University of South Australia, Mawson Lakes boulevard, Mawson Lakes, South Australia 5095, Australia

[3]Departament d'Enginyeria Mecànica, Universitat Rovira i Virgili, Av. Països Catalans 26, 43007 Tarragona, Spain.

*Corresponding author: alvaro.degracia@urv.cat

Abstract

Photovoltaic panels (PV) coupled to a heat pump supplying heat to a radiant wall is a system with potential to reduce the imported energy from the grid for heating and cooling of buildings. The radiant wall works as a thermal storage system (TES) allowing storage of the PV output and, thus, peak load shifting. However, the management of these technologies is complex, due to the dynamics of the system. This paper presents several control concepts with different purposes such as shifting energy use to off-peak periods, maximizing self-consumption of PV output, and minimization of imported energy from the grid. An experimentally validated numerical model from previous research was used to investigate and compare the different proposed control concepts. Results showed that charging the wall with solar energy resulted in higher overall energy use of the heat pump, while the imported grid energy was significantly reduced, thanks to self-consumption.

Keywords: radiant wall, photovoltaic panels, simulation, control concept

Nomenclature

TABS	Thermally activated building systems
PV	Photovoltaic panels
TES	Thermal energy storage

FVM	Finite volume model
COP	Coefficient of performance

Parameters		Sub-index	
T	Temperature (ºC)	as	Assumed
P_{PV}	Output power of PV array (W)	calc	Calculated
R	Thermal resistances ($K \cdot W^{-1}$)	i	Surface
Ɛ	Emissivity (-)	i-j	Heat transfer between surfaces
A	Area (m^2)	rad	Radiation
G	View factor (-)	conv	Convection
q	Heat flux (W)	load	Cooling load
X	Thermal resistances matrix ($W \cdot K^{-1}$)	inv	Inverse matrix
Y	Temperature gradient matrix (K)	(i,j)	Position in the matrix
Z	Heat flux matrix (W)	out	Outdoor
I	Infiltrations (% of air exchange per time step)	in	Indoor
ρ	Density ($kg \cdot m^{-3}$)	star	Star node
c_p	Specific heat capacity ($J \cdot kg^{-1} \cdot K^{-1}$)		
V	Volume (m^3)		
Δt	Time step (s)		
t	Time (s)		
h	Convective heat transfer coefficient ($W \cdot m^{-2} \cdot K^{-1}$)		
rf	Relaxation factor		

1. Introduction

Buildings are widely known as global major energy consumers and greenhouse gas emitters, with 32 % of global energy use [1] and 36 % of overall CO_2 emissions [2]. This issue is tackled by the European Directive 2010/31/EU [3] and it is also present in Paris COP 21 agreements [4]. The first step to solve this problem requires improving energy efficiency in buildings by improvement of envelopes, management of solar gains, and reduction of internal loads, among others. However, the final objective is to achieve net-zero energy buildings or even net-positive energy buildings [3], meaning that buildings should at least produce the same energy they consume. This implies integration of renewable energy into buildings, however the mismatch between availability of renewable energy and building energy demand profiles also requires energy storage systems.

Thermally activated building systems (TABS) have been widely studied for their potential to reduce energy use of buildings for space heating and cooling [5-8]. TABS consist of pipes or ducts embedded into the building structure, such as floors, ceilings, walls, and in-floor slabs. As a result, TABS make use of the availability of big internal surface in the building, which allows fulfilling the heating or cooling demands at reduced gradients between the fluid supply temperature and the indoor space temperature. As a result, TABS can operate with lower supply temperature for heating or higher supply temperature for cooling [5]. This is useful to increase the efficiency of heating and cooling systems or to integrate renewable energy sources, for example, free-cooling with ground heat exchangers [9] or night cool air [10]. Moreover, the fluid circulating through the pipes or ducts directly exchanges heat with the building structure and, thus, the building thermal mass is actively used for energy storage. Consequently, TABS can be considered as a short term, sensible, and low temperature thermal energy storage (TES) technology characterized as being actively charged and passively discharged. The storage capacity of TABS further increases their capability for integration of renewable energies through peak load shifting.

A promising system for integration of renewable energy in heating and cooling consists of photovoltaic panel (PV) arrays feeding heat pumps coupled to a TES system. The solar power produced is used for heating, cooling, or other electrical-consuming appliances. However, when PV output is higher than the building energy demand, the excess energy is not sold to the grid but used to charge a TES through the heat pump. Regarding this system working in heating mode, a simulation study of photovoltaic thermal array (PVT) coupled to a ground source heat pump and a water tank showed that the system provided 96 % of the electrical demand and fulfilled all heat demand [11]. A similar project determined the PV surface required to achieve a net-positive building in a system without a storage tank but a radiant floor [12]. The control of this system was also studied. A model predictive control (MPC) showed an improved performance in a system using high-mass radiant floor together with a TES tank [13]. The same control model showed a 45 % energy saving in a similar set-up [14]. This system was also applied for cooling, showing different economic opportunities in Brazil [15]. Additionally, its implementation into industrial buildings was also studied, with results indicating economic potential of exploiting PV output or off-peak periods [16]. All of these studies aimed towards net-zero or net-positive energy buildings and most considered some kind of TES [11,13,14,16]. However, most of them considered that the PV electrical power output fulfilled the electricity demand by using the grid as energy storage.

Furthermore, several studies considered some kind of TABS in the form of radiant heating floors [11-14], but only one considered it as a TES system [14].

A challenging topic to overcome for a wide implementation of TABS is the control. The management of the low response time and the peak load shifting capability require control strategies that take into account the dynamics of the system. Moreover, controlling TABS implies defining the supply temperature, the flow, and the ON/OFF criterion, which involves defining the duration of the active period. Usually the supply temperature is regulated by a heating/cooling curve dependant on outdoor conditions [17], although constant supply temperature is also used. On the other side, the simplest strategy for ON/OFF are set-back controls, in which a set-point temperature is maintained with a dead band regulating the temperature at which the system turns ON or OFF [18]. Both heating/cooling curves and set-back are reliable and robust controls, however, optimization of TABS operation requires more advanced controls. As a result, TABS were studied coupled to gain scheduling control (GSC) [19], pulse width modulation (PWM) [20], adaptive predictive control [21], and MPC [13,22], among others, all showing improved performance compared to common base case controls. Finally, MPC was highlighted as a control scheme with good potential for optimizing TABS operation, although further research is needed [8].

The current paper presents a study of the control concepts for a system consisting of a radiant wall supplied by a heat pump coupled to a PV array. The main objective was to minimize the cost for space cooling of a building, and thus the peak load shifting capacity of the radiant wall was used for operation during off-peak periods or for charging during periods with availability of solar energy. Here, the only storage system was the radiant wall itself, which was considered as a short term TES. The research was carried out by simulating the performance of the system under different control concepts which gave guidelines of the best way to operate the system for reducing cooling cost.

In order to develop the study, a numerical model was developed for a simplified cubicle exposed to outdoor conditions. These approach was based in previous experimental research on radiant wall cubicle, which showed good energy savings potential and peak load shifting capability [24,25]. From this experimental research, a numerical model of the radiant wall was validated [26] and then implemented in the current research.

2. Model description

In previous research, a 2D transient finite volume model of a radiant wall was developed and experimentally validated [26]. However, this model only described the behaviour of the radiant wall, which required, among other inputs, the indoor temperature. In order to study control strategies a cooling demand was required, consequently a building model had to be implemented. In the research of the current paper a simplified model of a cubicle, a room without openings, was used. This had internal size of 5.25 x 2.7 x 2.7 m (surface of 14.175 m^2) with radiant walls in all the walls, and without windows. All the walls were exposed to outdoor conditions. These approach was based on the knowledge obtained in previous experimental research of a radiant wall cubicle [24,25]. The collected data was used for verifying the reliability of the room model.

The following sections describe the details of the cubicle model, the associated components, and the calculation algorithms.

2.1. Cubicle model

The cubicle was modelled using a six surface star-network according to the methodology proposed by Seem [28]. This modelling simplifies actual radiation and convection heat transfer processes in the room avoiding the manipulation of polynomial matrices required when view factors are used to model long-wave radiation. Seem [28] presented a computationally easy method for transforming the view factor scheme, shown in Figure 1, into the star-network scheme shown in Figure 2. The star node represents a fictitious temperature that channels the radiation heat transfer between surfaces and the convection heat transfer between the surfaces and the indoor air.

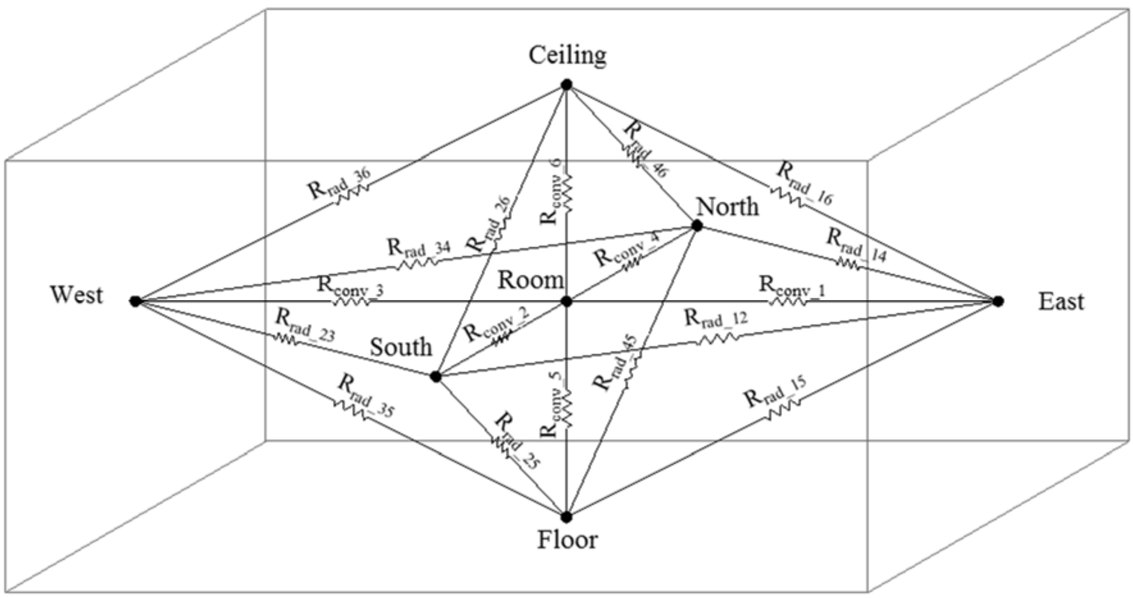

Figure 1. View factors heat transfer scheme (note radiation resistances between opposite surfaces could not be represented)

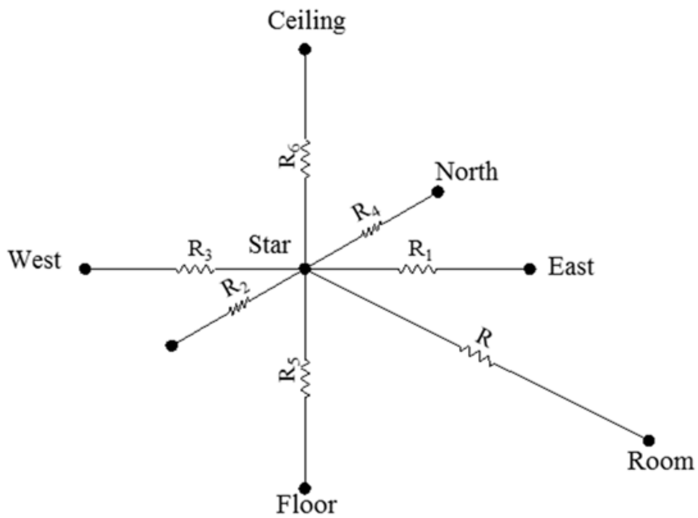

Figure 2. Star-network scheme for six surfaces

The view factor matrix convection resistances ($R_{conv,i}$) were calculated using the convection factors of UNE-EN ISO 6946 for indoor surfaces; note that this standard proposes a mixed convection and radiation factor, but in this paper $R_{i,c}$ was calculated only with the convection part, as the model considered radiation independently.

The radiation between surfaces was represented with $R_{rad,i-j}$, which was calculated with equation (1) [29].

$$R_{rad,i-j} = \frac{1}{\varepsilon_i \cdot A_i \cdot G_{i-j} \cdot \sigma \cdot 4 \cdot \bar{T}}$$

(Eq. 1)

where ε_i was emissivity, A_i area, G_{i-j} view factor between surfaces, σ Stefan-Boltzmann constant, and $\bar{T}$ was calculated with equation (2). Note that actual view factors were used.

$$\bar{T} = (T_i + T_j) \cdot (T_i^2 + T_j^2)$$

(Eq. 2)

According to Seem, the energy balances on each surface and in the room could be combined into matrix equations with the following form:

$$X \cdot Y = Z$$

(Eq. 3)

where Y and Z are the temperature gradient and heat flux matrixes respectively, which are shown in Table 1. On the other side, X matrix is conductivity matrix and is presented in Table 2.

Table 1. Y and Z matrixes

	Y		Z
Y=	$(T_1 - T_{in})$	Z=	$-q_1$
	$(T_2 - T_{in})$		$-q_2$
	$(T_3 - T_{in})$		$-q_3$
	$(T_4 - T_{in})$		$-q_4$
	$(T_5 - T_{in})$		$-q_5$
	$(T_6 - T_{in})$		$-q_6$
	q_{load}		0

Table 2. Matrix X

$-\left(\sum_{\substack{j=1 \\ j \neq 1}}^{6} \frac{1}{R_{rad,1-j}}\right) - R_{conv,1}$	$\frac{1}{R_{rad,1-2}}$	$\frac{1}{R_{rad,1-3}}$	$\frac{1}{R_{rad,1-4}}$	$\frac{1}{R_{rad,1-5}}$	$\frac{1}{R_{rad,1-6}}$	$\frac{1}{R_{conv,1}}$
$\frac{1}{R_{rad,2-1}}$	$-\left(\sum_{\substack{j=1 \\ j \neq 1}}^{6} \frac{1}{R_{rad,2-j}}\right) - R_{conv,2}$	$\frac{1}{R_{rad,2-3}}$	$\frac{1}{R_{rad,2-4}}$	$\frac{1}{R_{rad,2-5}}$	$\frac{1}{R_{rad,2-6}}$	$\frac{1}{R_{conv,2}}$
$\frac{1}{R_{rad,3-1}}$	$\frac{1}{R_{rad,3-2}}$	$-\left(\sum_{\substack{j=1 \\ j \neq 1}}^{6} \frac{1}{R_{rad,3-j}}\right) - R_{conv,3}$	$\frac{1}{R_{rad,3-4}}$	$\frac{1}{R_{rad,3-5}}$	$\frac{1}{R_{rad,3-6}}$	$\frac{1}{R_{conv,3}}$
$\frac{1}{R_{rad,4-1}}$	$\frac{1}{R_{rad,4-2}}$	$\frac{1}{R_{rad,4-3}}$	$-\left(\sum_{\substack{j=1 \\ j \neq 1}}^{6} \frac{1}{R_{rad,4-j}}\right) - R_{conv,4}$	$\frac{1}{R_{rad,4-5}}$	$\frac{1}{R_{rad,4-6}}$	$\frac{1}{R_{conv,4}}$
$\frac{1}{R_{rad,5-1}}$	$\frac{1}{R_{rad,5-2}}$	$\frac{1}{R_{rad,5-3}}$	$\frac{1}{R_{rad,5-4}}$	$-\left(\sum_{\substack{j=1 \\ j \neq 1}}^{6} \frac{1}{R_{rad,5-j}}\right) - R_{conv,5}$	$\frac{1}{R_{rad,5-6}}$	$\frac{1}{R_{conv,5}}$
$\frac{1}{R_{rad,6-1}}$	$\frac{1}{R_{rad,6-2}}$	$\frac{1}{R_{rad,6-3}}$	$\frac{1}{R_{rad,6-4}}$	$\frac{1}{R_{rad,6-5}}$	$-\left(\sum_{\substack{j=1 \\ j \neq 1}}^{6} \frac{1}{R_{rad,6-j}}\right) - R_{conv,6}$	$\frac{1}{R_{conv,6}}$
0	0	0	0	0	0	-1

Finally, according to the method, the resistances of the star-network were calculated with equation 4 and equation 5:

$$R = \frac{\sum_{j=2}^{N} \sum_{i=1}^{j-1} \frac{R_{i-r}+R_{j-r}-R_{i-j}}{R_{i-j}^{3}}}{\sum_{j=2}^{N} \sum_{i=1}^{j-1} \frac{1}{R_{i-j}^{3}}}$$

(Eq. 4)

$$R_i = R_{i-r} - R$$

(Eq. 5)

where R_{i-r} and R_{i_j} were obtained from the inverse matrix of X as shown in equation 6 and equation 7, respectively:

$$R_{i-r} = -x_{(i,i),inv}$$

(Eq. 6)

$$R_{i-j} = x_{(i,j),inv} + x_{(j,i),inv} - x_{(i,i),inv} - x_{(j,j),inv}$$

(Eq. 7)

Finally, q_{load} accounted for the accumulated heat in the room air plus the internal loads and the infiltration loses, as presented in equation 8:

$$q_{load} = \rho \cdot cp \cdot V \cdot \frac{T_{in} - T_{in}^{t-1}}{\Delta t} + I \cdot \rho \cdot cp \cdot V \cdot (T_{in} - T_{out}) - q_{in}$$

(Eq. 8)

where I was infiltration in air changes per time step and q_{in} the internal gains. Then the q_{load} matches with the heat flux between star node and indoor air node, as shown in equation 9.

$$q_{load} = \frac{(T_{in} - T_{star})}{R}$$

(Eq. 9)

The resistance values were calculated at each iteration as they depend on temperature. Once those were calculated, the star temperature (T_{star}) and the indoor temperature (T_{in}) were calculated according to the energy balances. The input values were the temperatures of the indoor surfaces, the outdoor temperature, the internal gains, and the indoor temperature of the previous step. The heat flow on each surface was used to verify the energy balance of the room model and to compare it to the energy balances of the walls.

2.2. Radiant walls model

The radiant wall was composed of a 195 mm thick brick, 60 mm expanded polystyrene insulation, and a finishing layer of 5 mm fibrocement board on the outdoor surface, which resulted in a steady-state transmittance (U-value) of 0.5 $W \cdot m^{-2} \cdot K^{-1}$. The radiant system was obtained by 16 mm diameter pipes embedded spaced 150 mm and 36 mm deep from the indoor surface of the wall.

The radiant walls are modelled with a 2D transient FVM model described in Romaní et al. [26]. However, the boundary conditions on the indoor surface of the radiant wall model were not compatible with the requirements of the cubicle model. The FVM of the radiant wall model used the combined radiation and convention heat transfer coefficient obtained according to UNE-EN ISO 6946 [27], in which the convection heat calculated using the newton equation accounts for both convection and radiation, as shown in equation (10) were h_c was a constant that depended on the orientation of the surface and the heat flux, ε was the emissivity , and T_m was the average thermodynamic temperature on the surface. In contrast, the star-network model of the room takes into account the actual radiation heat transfer between the surfaces, by taking in account the view factors. Moreover, once transformed to star-network, the surfaces of the room model exchange heat with the star node, while the FVM exchanges heat with the indoor temperature.

$$h_{comb} = h_c + \varepsilon \cdot 4 \cdot \sigma \cdot T_m^3$$

(Eq. 10)

In order to match the cubicle model, the boundary condition on the indoor surface of the wall was modified to a heat exchange with T_{star} with a heat transfer equivalent to the surface resistances of each wall in the star-network, as shown in equation (11):

$$h_{int} = \frac{1}{R_i \cdot A_i}$$

(Eq. 11)

The cubicle model assumed average surface temperature for each wall. However, the FVM model calculated a temperature profile on the indoor surfaces. Therefore, the results of the radiant wall temperature were summarized to an average surface temperature, in which each node temperature was weighted according to its surface.

Moreover, as the room model needed uniform surfaces, the whole surface of the radiant walls was considered to have embedded pipes. In order to match this assumption, the length of piping in the radiant walls was calculated proportionally to the wall surface area. The FVM had a definite pipes-to-wall ratio, which was used to calculate the total pipe length. This calculation was required to accurately obtain the heat flux required to the heat pump in order to achieve the adequate cooling at the walls surface.

2.3. Floor and roof model

The floor was modelled together with the ground in a mixed FVM mesh. The ground was modelled as 1D, with the under-ground boundary temperature calculated with Joan & Baggs equation [31]. Then, the concrete base of the cubicle was modelled as 2D, representing the slab from North to South. The boundary conditions considered that all the nodes at the bottom of the slab exchanged heat to the single node of the ground. The nodes exposed to outdoors had convective heat exchange with outdoor air. Furthermore, the horizontal surface exposed to outdoor on the south had incident solar radiation, while the north surface was considered to be in the shadow. On the other side, the nodes below the walls considered this boundary as adiabatic, as no heat exchange with walls was considered. Finally, nodes on the indoor surface exchanged heat with T_{star} in the same way as the walls, and thus using also equation 10. Furthermore, for the calculation of the room temperature, the floor temperature was considered as a uniform value equivalent to the average node temperatures, weighted by surface area.

The roof model consisted in 1D transient FVM. The model was solved explicitly to reduce the computational effort. On the outdoor surface the model considered convective heat exchange with outdoor air, incident horizontal solar radiation, and long-wave heat exchange with the sky. The long wave radiation was calculated with the radiosity and irradiosity method, assuming sky temperature according to the Swinback correlation [30]. On the indoor surface the roof exchanges heat against T_{star} with a heat transfer coefficient obtained from the star network (R_i).

2.4. *Heat pump model*

Several assumptions were taken into consideration for the heat pump modelling. First, the supply temperature to the walls was constant at 15 ºC, assuming a temperature gradient in the evaporator of 5 K, which resulted in an evaporator temperature of 10 ºC. With these assumptions, the COP of the heat pump was modelled as a regression curve of the values provided by a manufacturer [32] for a LH33E/2GES-2Y-40S compressor. The COP is provided depending on the outdoor temperature at a specific evaporator temperature, including the fan power. The regression curve obtained is shown in Figure 3. Finally, the total electrical energy use of the heat pump was calculated with the calculated COP and the heat flux in the radiant walls at each time step.

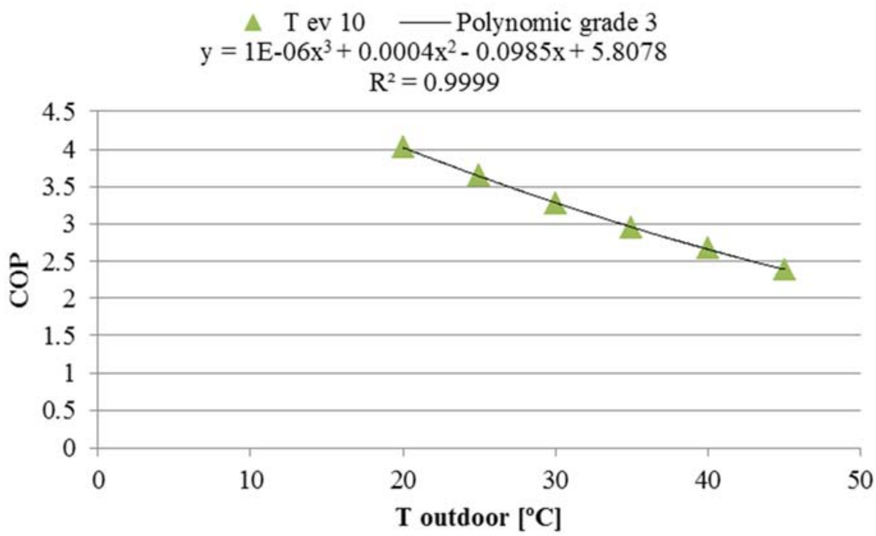

Figure 3. Heat pump COP curve at evaporator temperature 10 ºC

2.5. *Model of PV panels*

The PV panels were simplified by assuming a constant efficiency of 15 %, and thus the electricity supplied was a constant fraction of the incident global solar radiation. This study considered 6 panels of 1.68 m^2 each, placed horizontally. The total nominal power of installed PV was equivalent to 1512 W.

2.6. *Internal gains*

The internal gains introduced in the model represent domestic occupancy. It takes into account the high activity periods of occupants in the early morning and afternoon, the occupancy with low activity at night, and non-occupancy during the day. Minimum internal loads were used during non-occupancy in order to represent the heat generated by appliances. As a result, the heat loads profiles had 15 $W \cdot m^{-2}$ from 6 am to 9 am and from 5 pm to 10 pm, 7.5 $W \cdot m^{-2}$ from 10 pm to 6 am, and 3.75 $W \cdot m^{-2}$ from 9 am to 5 pm. The daily distribution of the internal gains is shown in Figure 4.

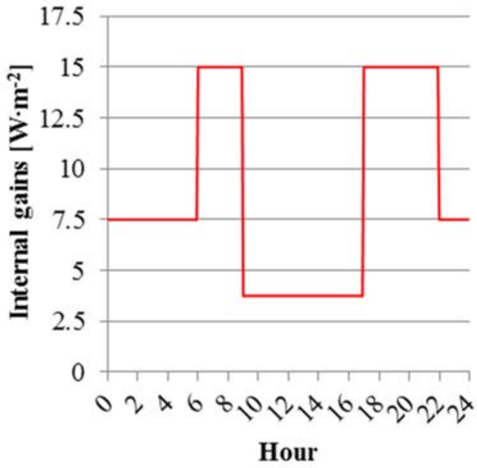

Figure 4. Domestic daily internal gains schedule used in this study.

2.7. Algorithm of calculation

The algorithm used by the model requires iteration for each time step as shown in Figure 5. Each iteration first calculated the variable coefficients, such as the convective heat transfer coefficients or the resistance values of the star-network. Then the temperatures of the walls, floor, and ceiling were calculated, followed by the indoor temperature. Finally, the error between the calculated values and the supposed values at the start of the iteration was verified. If the error was higher than the maximum acceptable (10^{-6} K), a new iteration started. The supposed values were updated with the calculated values of the previous iteration taking into account a relaxation factor. The time step between iterations was 5 minutes.

In case the heat pump was "ON", at the start of each iteration a temperature gradient was supposed for the supply water in each wall. At the end of each iteration, the temperature gradient was updated with the heat flux calculated for each wall.

The status of the heat pump was checked at the beginning of each time step.

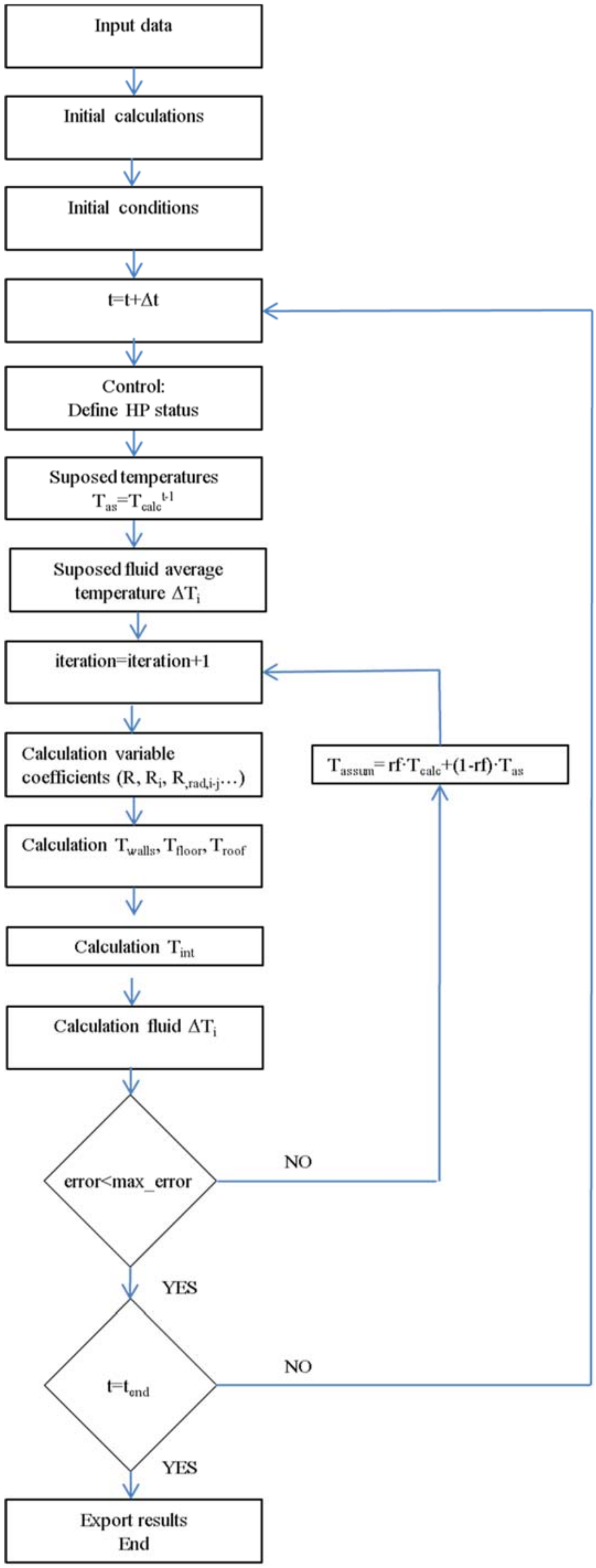

Figure 5. Model algorithm

3. Methodology

3.1. Description of control concepts

Six control concepts were applied into the management of the heat pump, such as solar basic, solar following, solar hybrid, solar predictive, and peak load shifting. The criterion defining each concept depended on different objectives. First, all concepts had to maintain the indoor temperature into the comfort range (21 ºC-26 ºC) all the time. Then, the different objectives were:

- To maximize the use of the energy produced by the PV panels.
- To minimize imported energy from the grid.
- To minimize imported energy from the grid in peak periods.
- To shift energy use to off-peak periods.

3.1.1. Operation modes

In order to achieve the objectives, each control concept used different operation modes of the heat pump, which are described in Table 3. The mode type define its objective, with "standard" type referring to maintaining the comfort conditions and "charging" type standing for storing energy to the cubicle with peak load-shifting purposes.

Table 3. Heat pump operation modes (*"Solar predictive" concept uses variable set-point for "pre-cooling" mode)

Mode	Type	ON criterion	OFF criterion	Notes
Comfort	Standard	$T_{in} > 26$ ºC	$T_{in} < 24$ºC	Always active unless another mode was ON
Solar	Charging	$T_{in} > 22$ ºC	$T_{in} < 21$ ºC	Only activated during daylight hours
Solar threshold	Charging	$T_{in} > 22$ ºC and $P_{PV} > 1500$ W	$T_{in} < 21$ ºC or $P_{PV} < 1500$ W	Only activated during daylight hours
Pre-cooling	Charging	$T_{in} > 22$ ºC*	$T_{in} < 21$ ºC*	Only activated in night off-peak periods

3.1.2. *No control concept*

The "no control" concept simply focused in maintaining the indoor temperature inside the comfort range, without taking into account any other inputs. This control concept only used the "comfort" operation mode. The scheme of the "no control" concept is shown in Figure 6.

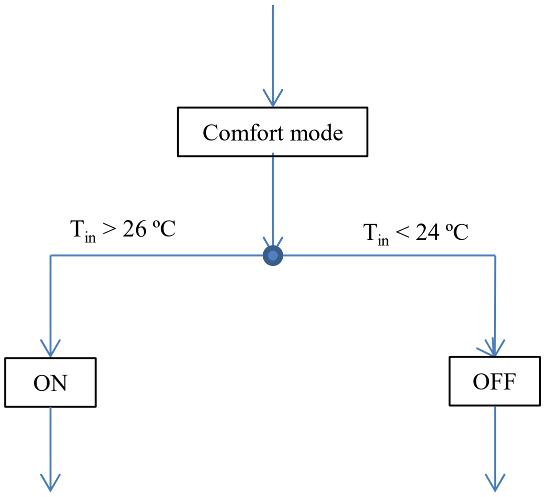

Figure 6. No control concept

3.1.3. *Solar basic concept*

The "solar basic" control modified the set-point temperatures during the daylight hours with the objective of maximizing the use of the energy produced by the PV panels. This concept had two operation modes depending on the time. On one side "comfort mode" was activated from 6 pm to 10 am. On the other side, "solar charging" mode was applied from 10 am to 6 pm. The scheme of the concept is shown in Figure 7.

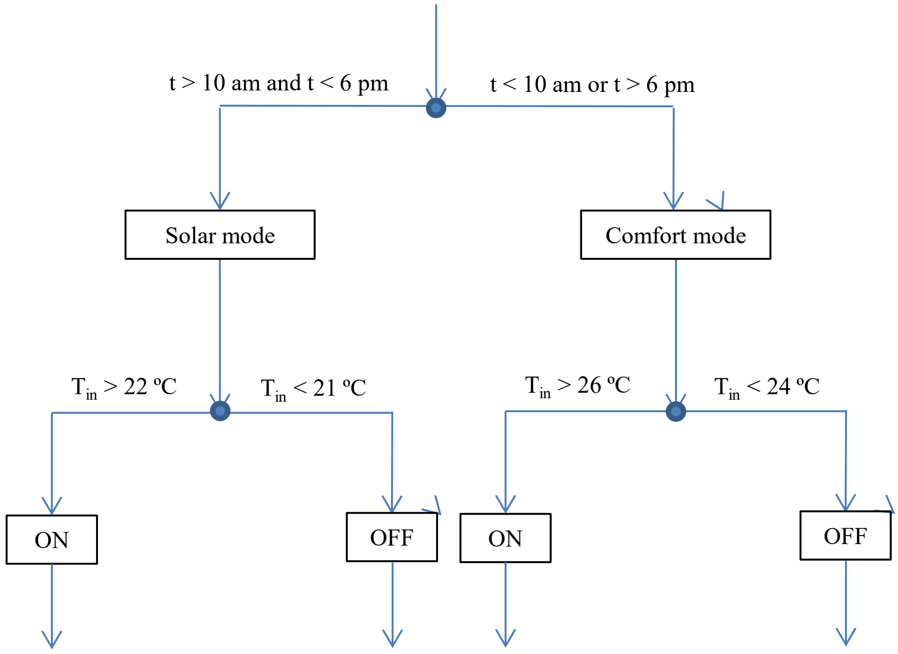

Figure 7. Solar basic control concept

3.1.4. Solar following concept

The "solar following" concept was a modification of the "solar basic control". In this case the actual power output of the solar panels was taken into account, activating "solar following" from 10 am to 6 pm. The objective of this modification was to minimize the imported energy from the grid, as the concept required a solar output higher than the average power of the heat pump. If the power output was insufficient, the control stayed in the "comfort" mode. The scheme of the control is shown in Figure 8.

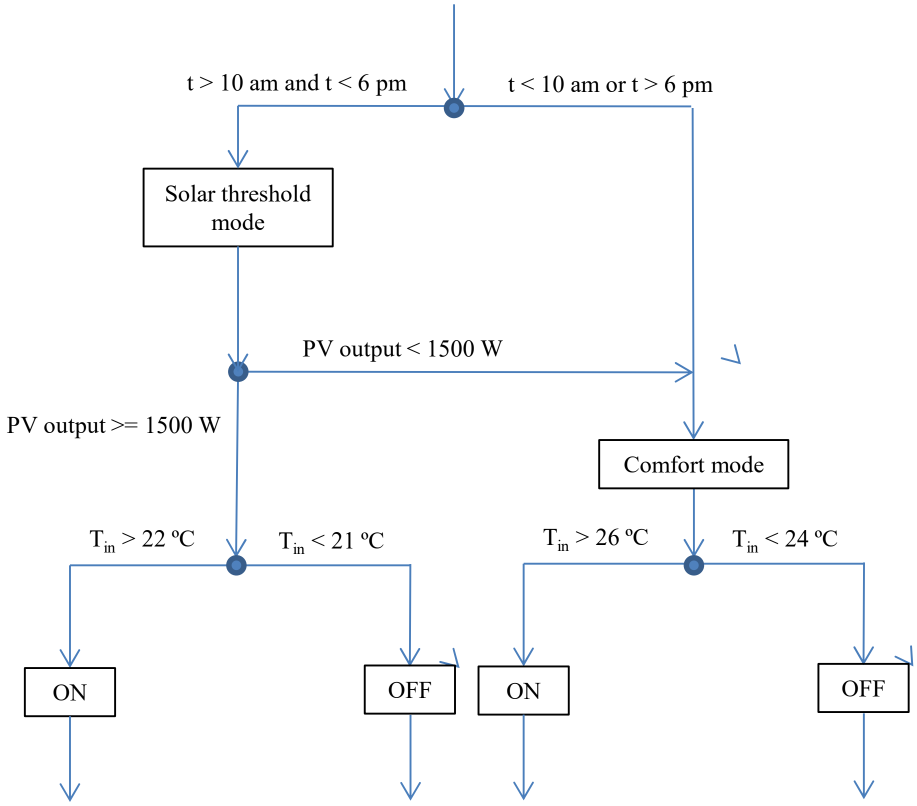

Figure 8. Solar following control concept

3.1.5. Solar hybrid concept

The solar hybrid concept had the objectives of maximizing the use of the energy produced by the PV panels and minimizing the imported energy in peak periods. In Spain, the change from off-peak to peak tariff is at 1 pm in summer. As a result, this concept operated in "solar" mode from 10 am to 1 pm, however, from 1 pm to 6 pm the concept operated in "solar following". In this way, the heat pump could charge the wall during off-peak hours, exploiting the output of the PV panels even if that was not enough to off-set the energy use of the heat pump. However, once in the peak period, beyond 1 pm, the wall was charged only if the solar power output was enough, and thus the solar output was exploited but importing energy was avoided. During the rest of the day the concept operated in "comfort mode". The scheme of the concept is shown in Figure 9.

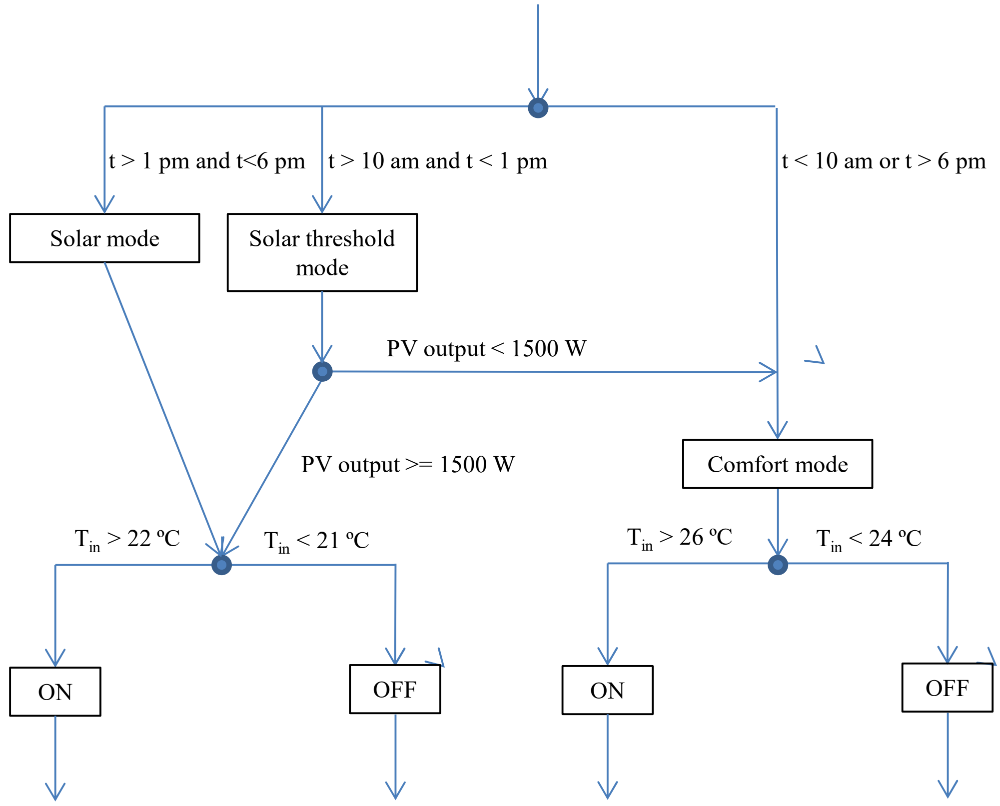

Figure 9. Solar hybrid control concept

3.1.6. *Solar predictive concept*

The objectives of the solar predictive control was to minimize the imported energy on peak periods, to maximize the use of the energy produced by the PV panels, and to shift energy use to off-peak periods. With these objectives, this concept had activated a modified "pre-cooling" mode in the early morning. In this period the control forecasted the expected solar radiation during the day, classifying it between "sunny", "partially sunny", "partially cloudy", and "cloudy". The day classification was done taking as reference the day with the highest accumulated solar radiation in the studied period, which was June 19th with a total accumulated radiation on a horizontal surface of 9.7 kWh·m^{-2}. Then, "sunny" was considered for days with accumulated solar radiation more than 75 % of this value, "partially sunny" for values between 50-75 %, "partially cloudy" for values between 25-50 %, and "cloudy" for values below 25 %. Each type of forecasted day had different set-points in the "pre-cooling" mode, as shown in Figure 10.

Moreover, during the daylight hours, from 10 am to 6 pm, the concept operated in "solar threshold" mode. The scheme of the concept is shown in Figure 10. This concept was applied with two different length of the pre-cooling, a 2 hours period from 5 am to 7 am, and a 4 hours period from 3 am to 7 am (referred as "solar predictive 2h" and "solar predictive 4h", respectively).

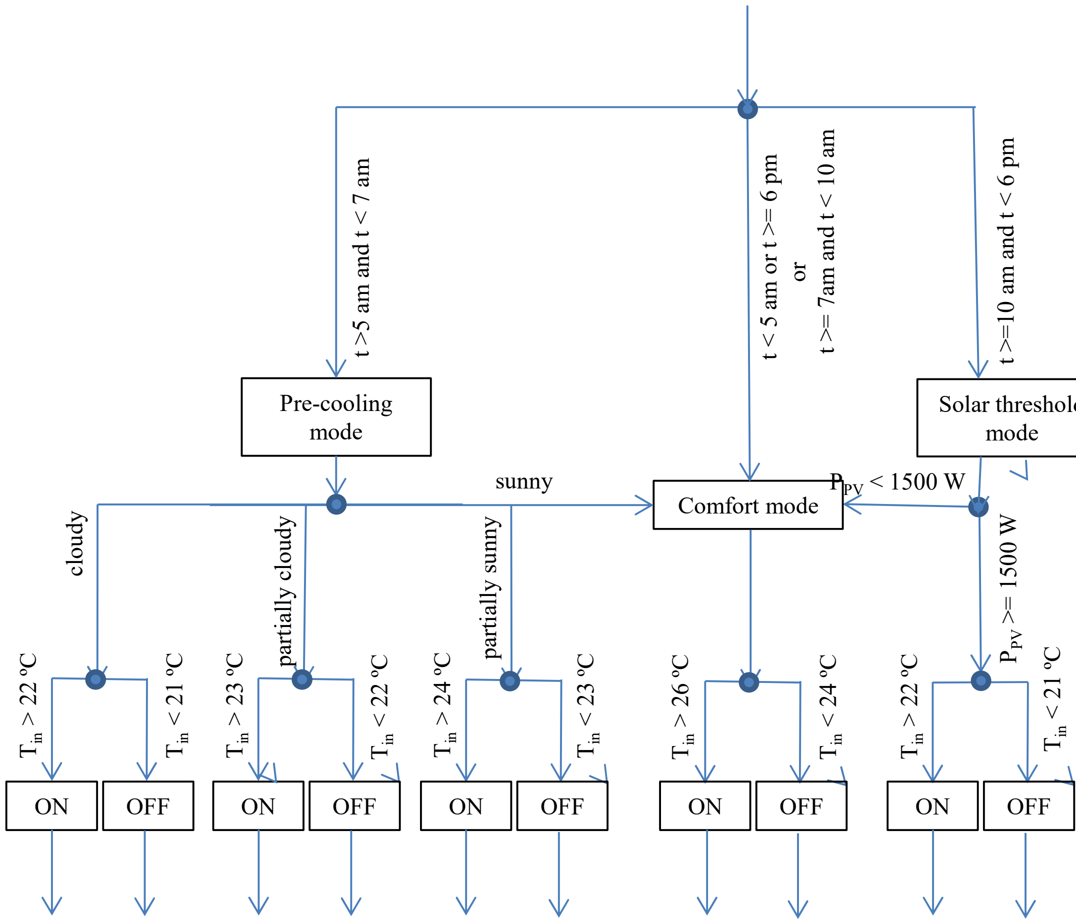

Figure 10. Solar predictive 2 h control concept

3.1.7. Peak load shifting concept

The objective of the peak load shifting concept was shifting the peak loads and minimizing the imported energy in peak periods. As a result, it used two operation modes, “comfort” mode and “pre-cooling” mode. Parallel to “solar predictive” concept, two different length of the pre-cooling period were used, a 2 hours period from 5 am to 7 am, and a 4 hours period from 3 am to 7 am (referred as “peak load shifting 2h” and “peak load shifting 4h”, respectively). The design of this concept is an approach contrary to exploiting the PV output, as the purpose was to consume all the energy during night-time.

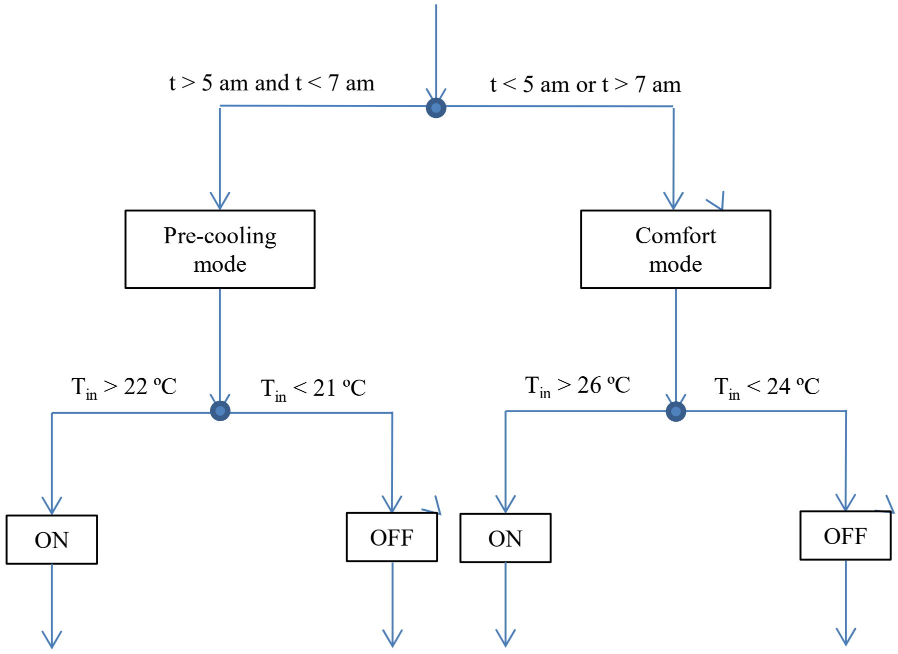

Figure 11. Peak load shifting 2 h concept

3.2. *Electricity cost*

Each electricity company in Spain offers different tariffs for domestic consumers, however, all tariffs take into account a peak and off peak period, which in summer peak time is from 1 pm to 11 pm. The differences between domestic tariffs are on the calculation method of the price, however, all tariffs offer incentive for the energy use in the off-peak period. A reference tariff was used in the study [33], this had a different energy cost in peak and off-peak periods, with constant power term as shown in Table 4. As the power term was constant and the research did not influence this parameter, only the energy cost was considered.

Table 4. Domestic electric tariff summary

Power term	Peak time	Peak Cost	Off peak time	Off peak cost
€/kW		€/kWh		€·kWh^{-1}
3.17	1 pm to 11 pm	0.147675	11 pm to 1 pm	0.067255

On the other side, Spain policies promote self-consumption of the energy produced with low export prices and a tax which is payable for injecting electricity to the grid. Moreover, this study did not consider other appliances that could consume the energy produced by the PV panels. Therefore, the excess energy not consumed by the heat pump was disregarded.

3.3. *Weather data*

The simulations were carried out for a whole summer from May 1st to September 30th. The data were obtained from the experimental test site located at Puigverd de Lleida (Spain), whose coordinates are 41.56 N, 0.74 E. The region is considered as a hot summer and mild cold winter climate, labelled as Csa according to Köppen-Geiger [34] classification. The outdoor temperature was measured with ELEKTRONIL EE21 transducer and the solar radiation was measured with a Middleton solar pyranometer, all measurement were taken in a 5 minutes time interval.

4. Results

The performance of each control concept was evaluated according to the energy use, the operation cost, and the thermal comfort.

4.1. *Energy use*

The energy use for all control concepts is presented in Figure 12. The simulation results showed that all "solar" control concepts used overall more energy than "no control" or "peak-load shifting" concepts. This was caused by "solar" concepts having longer periods at low set-point, and thus higher cooling load. However, "solar" concepts had low imported energy when considering that the heat pump directly consumed the energy provided by the PV panels.

Among the "solar" concept, the criterion of activating the heat pump only if enough power was supplied by the PV resulted in less overall energy use but in higher imported energy. This was caused by the limited available power from the PV panels, which only had short periods providing more than 1500 W. As a result, "solar following" and "solar predictive" control concepts activated the charging mode for less time, consuming less energy. However, as fewer cooling was provided during the day time, a cooling demand was generated when internals gains kicked in at the afternoon. Then the heat pump was activated according to "comfort" mode, but without PV output available all the energy had to be imported in peak period. On the other side, "solar hybrid" had an energy use between "solar basic" and "solar following" concepts. However, once considering self-consumption "solar hybrid" had less energy use. A further advantage of "solar hybrid" was that all imported energy was consumed in off-peak periods, as shown in Figure 13. Consequently "solar hybrid" had both the least imported energy and the least peak energy use.

Furthermore, few differences were observed between "solar following" and "solar predictive" concepts regarding overall energy use. This was mainly caused by the criterion defining the type of days. Despite the control identified more than 25 % of days as non-sunny, and thus requiring pre-cooling, the actual heat gains and indoor temperatures did not trigger the activation criterion for the heat pump, as the indoor temperatures were already lower than the defined set-point. Consequently, the energy use of "solar following" and "solar predictive" was mainly driven by the "solar threshold" mode, which was common in both concepts. However, when considering the distribution of the energy use, the "solar predictive" concept had more imported energy. This was the result of the pre-cooling periods, which increased the energy use. In contrast, the pre-cooling shifted the imported energy use to off-peak periods, resulting in "solar predictive" having less peak energy use than "solar following", as shown in Figure 13.

On the other side, "no control" and "peak load shifting" concepts had similar energy use, as shown in Figure 12. However, peak load shifting concepts concentrated the energy use in off-peak periods. Moreover, the "pre-cooling" mode schedule resulted in "peak load shifting" concepts not exploiting the energy provided by the PV panels, therefore, importing almost all energy from the grid. Furthermore, the different length of the pre-cooling period only resulted in a slight increase in energy use. Otherwise, the longer period nearly guaranteed all energy use in off-peak periods. In cooling mode, the low outdoor temperatures during the night period avoided heat gains, therefore, once the set-point was achieved, the room did not had further cooling demand. Consequently, the set-point was the parameter for regulating the cooling required.

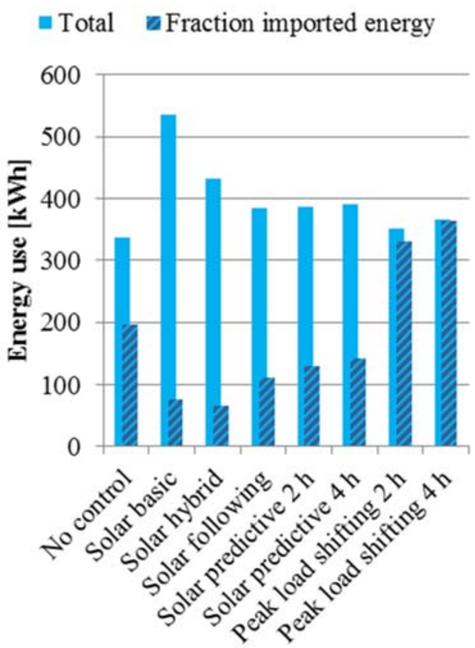

Figure 12. Total energy use and fraction of imported energy (all summer)

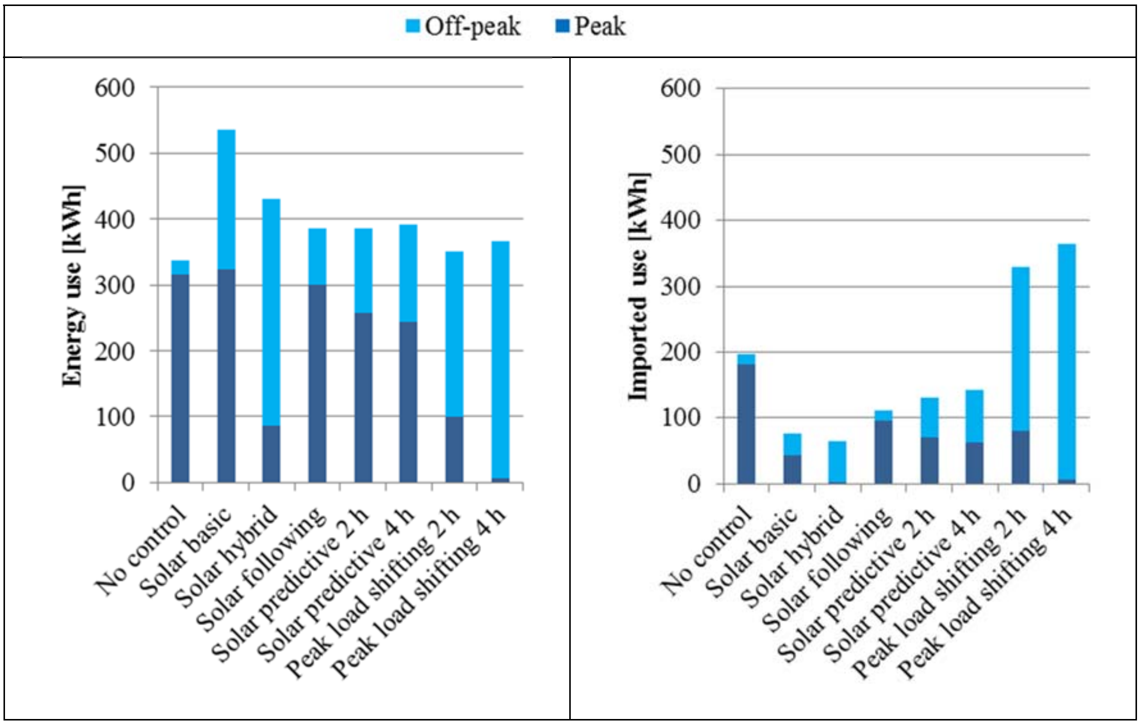

Figure 13. Total peak and total off-peak energy use (left) and imported energy (right) (all summer)

4.2. <u>Operation cost</u>

The operation costs for all control concepts are shown in Figure 14. The results are presented considering self-consumption of the PV energy output for "solar" and "no control" concepts (blue columns), although "no control" and "peak load shifting" concepts without self-consumption are shown as reference (red columns). These show that the "solar" concepts had the lowest operation cost, as a small amount of energy was imported from the grid as presented previously in Figure 13. Furthermore, as summarized in Table 5, all control concepts reduced the operation cost with self-consumption, despite this, "peak load shifting" concepts barely reduced their operation cost while "no control" reduced the cost much less than "solar" concepts. Once considering self-consumption all "solar" concepts showed high cost savings, especially the "solar hybrid" concept. Finally, the results showed that installation of PV panels was only exploited with "solar" type of control concepts. “Peak-load shifting” concepts without PV achieved similar operation cost or lower than “no control” concept with PV, therefore, the former had lower investment cost and could also achieve lower operation costs.

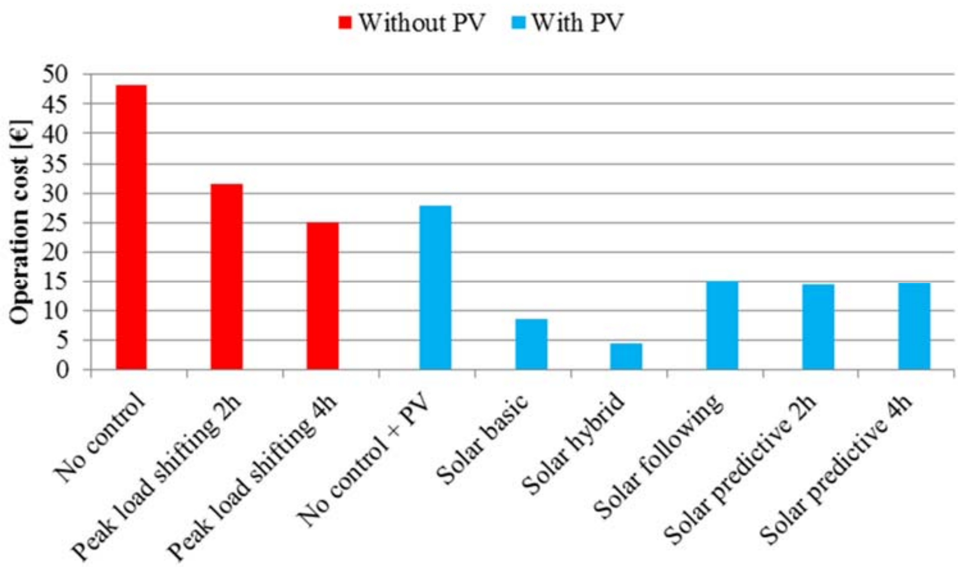

Figure 14. Operation cost with and without self-consumption (all summer)

Table 5. Operation cost with self-consumption per control concept (all summer)

Control concept	Operation cost with self- consumption (€)	Control concept cost difference without and with self-consumption PV	Cost compared to “no control” with self-consumption
No control	27.87	-42.13 %	--
Solar basic	8.62	-86.12 %	- 69.08 %
Solar hybrid	4.52	-87.38 %	- 83.76 %
Solar following	15.17	-69.68 %	- 45.56 %
Solar predictive 2 h	14.38	-69.23 %	- 48.40 %
Solar predictive 4 h	14.62	-68.19 %	- 47.52 %
Peak load shifting 2 h	28.60	-9.44 %	+ 2.64 %
Peak load shifting 4 h	25.02	-0.44 %	- 10.22 %

4.3. *Heat pump status*

The differences in energy use and operation cost of the "solar" control concepts can be further understood with the heat pump operation status shown in Figure 15. The results can be summarized as follows:

- "Solar basic" concept covered all cooling demand exclusively with "solar" mode, it did not require turning ON in the "comfort" mode.
- "Solar hybrid" mainly covered the cooling demand with "solar" mode. However, as this mode was limited up to 1 pm, the operation time of "solar hybrid" concept was lower than "solar basic". The remaining cooling demand was covered by "solar threshold" mode, resulting in "solar hybrid" concept not requiring activations in "comfort" mode.
- "Solar following" concept did not cover all the cooling demand with "solar threshold" mode, as the ON periods in this mode were restricted. Hence, it had to turn ON in "comfort mode", which was usually activated in off-peak periods during the afternoon.
- "Solar predictive" was similar to "solar following", however, part of the active time in "comfort" mode was shifted to "pre-cooling" mode, which led to lower operation cost.

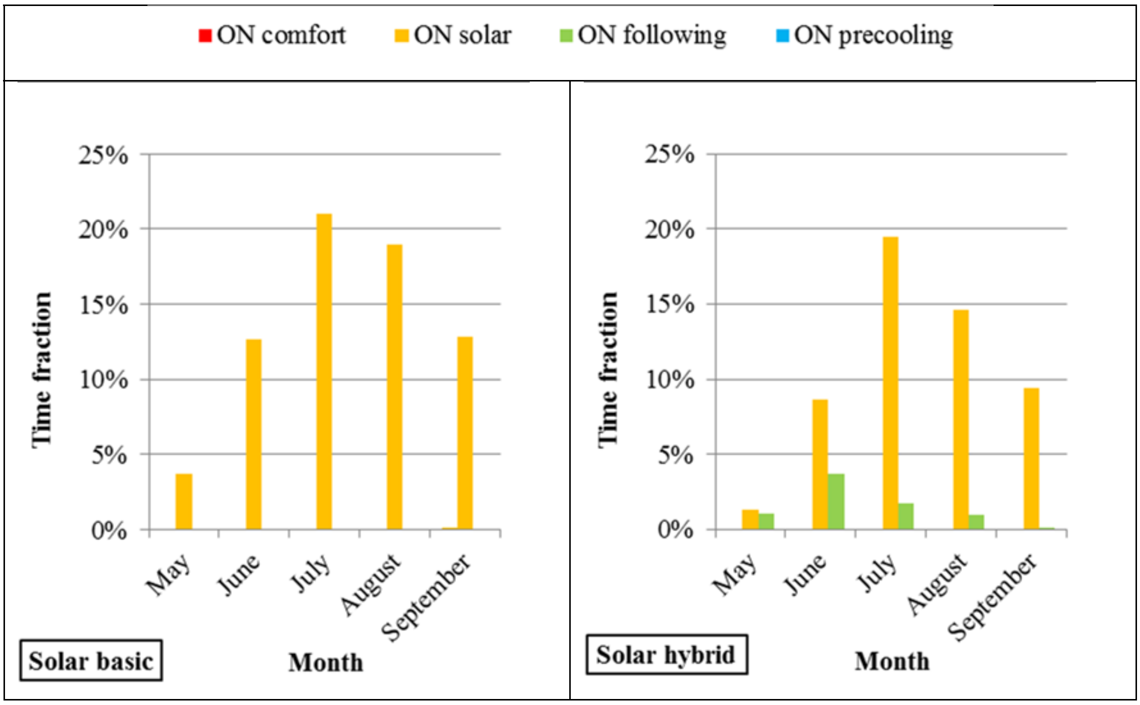

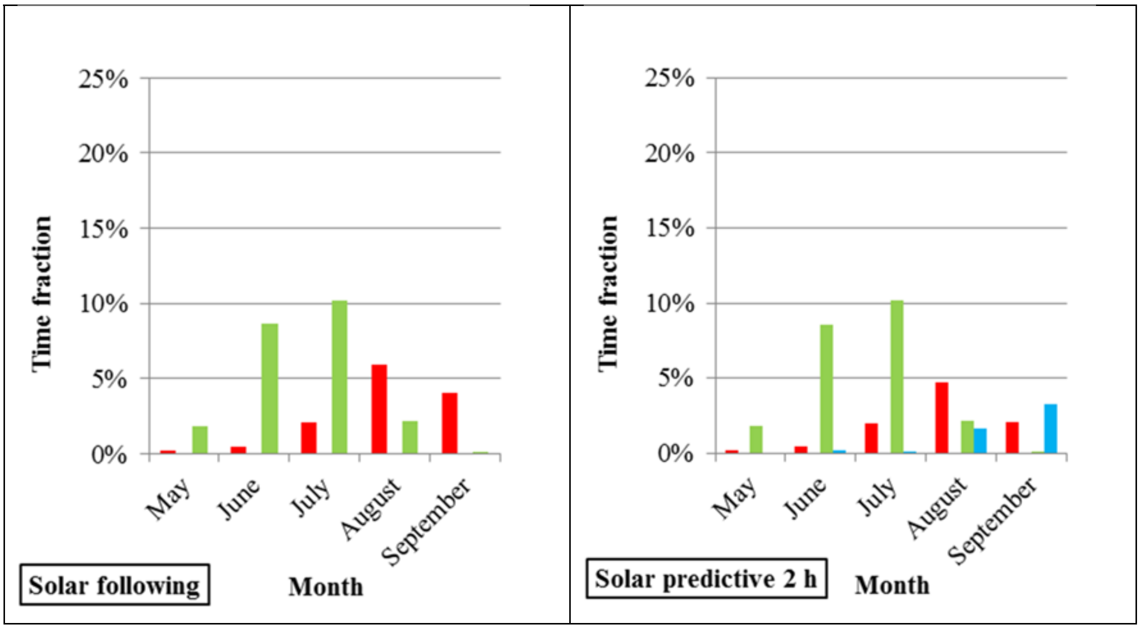

Figure 15. Time expended in each operation mode for solar control concepts

5. Discussion

The results of the study showed that the integration of radiant walls, heat pump, and PV could significantly reduce the imported energy form the grid. By using control concepts that charge the wall during daylight hours the system would increase the overall energy use, although, thanks to self-consumption the imported energy would be low.

With the studied set-up, the best control concept consisted of charging during daylight hours in off-peak periods without taking into account the actual solar output and then only charging during peak periods if the solar power output could cover the heat pump power demand ("solar hybrid" concept). This way the imported energy was low, moreover, all the imported energy was consumed in off-peak periods, and thus obtaining the lowest operation cost. However, a case with more PV installed capacity would favour a control concept in which charging is done when solar power output exceeds heat pump power demand ("solar following" concept), as it would guarantee zero imported energy while still having charging periods long enough.

The simulations showed the capability of the radiant wall as a TES system for storing the energy produced by PV through a heat pump. The control concepts presented focused in minimizing the imported energy by maximising the self-consumption of the PV output. This contrasted with research on net-zero or net-positive energy buildings, which usually considered the grid as the energy storage that overcame the mismatch between production and demand [11,12,15]. From a global point of view, this approach could result in an excess of power feed to the grid during noon, which would require expensive peak load shifting management at grid level that would result in higher energy cost. Consequently, focusing in maximizing self-consumption with building integrated TES, such as the radiant wall or other TABS, would both improve grid management and reduce operation cost for heating and cooling.

Despite the TES capability of the radiant walls was proven, the actual cooling performance could not be determined. Measuring the cooling supplied to the wall that actually cools down the indoor space does not reflect the behaviour of the system. While reducing the temperature resulted in an increase of the heat transferred to the wall from the outdoor space, it is also true that the radiant system acts a as thermal barrier, which reduces heat gains to the interior space. Furthermore, the focus of this research was to charge the wall with solar energy, and even with increased heat gains the operation cost and associated greenhouse emissions are very low. In the case studied here, the thermal efficiency of the radiant wall is a less relevant parameter compared to the increase of renewable energy use.

However, fully exploiting TABS storage capacity requires optimized controls. The literature presents extensive research on TABS control [6,8], among which predictive controls showed good synergy with TABS [8]. On this topic, the results on the studied control concepts offered guidelines towards improving predictive controls performance, by indicating the general control parameters to consider in the cost functions. Moreover, this paper presents an intuitive approach to best control, although it also highlights some key parameters to optimize such as indoor temperature set-point, PV output threshold for activating the heat pump, forecasting of PV output, expected cooling load and start/end time for charging periods. These parameters should be managed in order to minimize the operation cost and the imported energy while being constrained by the indoor temperature comfort range.

Furthermore, the presented research considered an air-to-water heat pump supplying at constant temperature and constant flow. Adjustment of these parameters could lead to a better performance of the heat pump [17], and consequently resulting in less overall energy use and operation cost. Moreover, using outdoor air as a heat sink meant a worse heat pump COP when charging during the day, as the outdoor temperature was higher. A ground source heat pump, free-cooling with ground heat exchanger, or evaporatively cooled condenser could improve the system performance in cooling mode, further increasing the advantage of "solar" concepts.

Finally, the results suggest moving away from the usual energy efficiency approach. The control concepts with less imported energy and operation cost were those consuming more overall energy. This is a common issue in peak load shifting with TES [16], which present benefits by increasing the renewable energy share although having higher overall energy use. In a context in which PV panels are getting cheaper [35] the feasibility of big PV arrays is higher, especially in single family houses. Consequently, solar electricity could be abundant, and thus the challenge will be to better exploit this energy, with energy efficiency being one parameter of the optimization process.

6. Conclusions

The control of a system consisting of radiant wall as TES for a heat pump coupled to a PV array was studied. Different control concepts were considered with the objective to reduce operation cost by peak load shifting, minimization of imported electricity from the grid, and maximisation of PV energy use. An experimentally validated model of a radiant wall was coupled to a simple room model that provided a base case for studying the behaviour of the different control concepts.

Charging the radiant wall with the solar energy output of a PV array through a heat pump resulted in a higher overall energy use. However, due to self-consumption of the produced energy the system imported little energy from the grid, resulting in a low operation cost.

The simulations also highlighted some parameters that could be optimized, such as indoor temperature set-point, PV output threshold for activating the heat pump, forecasting of PV production, expected cooling load and length and timing of charging periods.

The solar control concepts were promising references for reducing operation cost and minimizing imported energy. These were a solid base for the research of optimized control strategies of a radiant wall used as TES for a heat pump coupled to a PV array.

7. Acknowledgements

The authors acknowledge the South Australian Department of State Development who have funded this research through the Premier's Research Industry Fund - International Research Grant Program (IRGP 33). The work was partially funded by the Spanish government (ENE2015-64117-C5-1-R (MINECO/FEDER), ENE2015-64117-C5-3-R (MINECO/FEDER), and ULLE10-4E-1305). GREA is certified agent TECNIO in the category of technology developers from the Government of Catalonia. The authors would like to thank the Catalan Government for the quality accreditation given to their research group (2014 SGR 123) and the city hall of Puigverd de Lleida. This projects has received funding from the European Commission Seventh

Framework Programme (FP/2007-2013) under Grant agreement Nº PIRSES-GA-2013-610692 (INNOSTORAGE) and from European Union's Horizon 2020 research and innovation programme under grant agreement Nº 657466 (INPATH-TES). Alvaro de Gracia would like to thank Ministerio de Economia y Competitividad de España for Grant Juan de la Cierva, FJCI-2014-19940.

References

1. International Energy Agency, Energy Technology Perspectives 2012 Pathways to a clean energy System, 2012
2. European Commission, Technical Guidance-Financing the energy renovation of building with Cohesion Policy Funding, 2014
3. DIRECTIVE 2010/31/EU of European parliament and of the council of 18May 2010 on the energy performance of buildings (recast)
4. United Nations, Adoption of the Paris Agreement, Paris Climate Change Conference COP 21, UN, 2015
5. X. Xu, S. Wang, J. Wang, F. Xiao, Active pipe-embedded structures in buildings for utilizing low-grade energy sources: A review, Energy Build., 42 (2010) 1567–1581
6. J. Romaní, A. de Gracia, L.F. Cabeza, Simulation and control of thermally activated building systems (TABS), Energy Build., 127 (2016) 22-42
7. K.N. Rhee, B.W. Olesen, K.W. Kim, Ten questions about radiant heating and cooling systems, Build. Env. 112 (2017) 367-381
8. D. Olsthoorn, F. Haghighat, A. Moreau, G. Lacroix, Abilities and limitations of thermal mass activation for thermal comfort, peak shifting and shavings: A review, Build. and Env. 118 (2017) 113-127
9. J. Romani, G. Pérez, A. de Gracia, Experimental evaluation of a cooling radiant Wall coupled to a ground heat exchanger, Energy Build. 129 (2016) 484-490
10. R.A. Meierhans, Room air conditioning by means of overnight cooling of the concrete ceiling, ASHRAE Trans. 102 (1996) 693-69
11. M. Bakker, H.A. Zondag, M.j. Elswijk, K.J. Strootman, M.J.M. Jong, Performance and costs of a roof-sized PV/thermal array combined with ground coupled heat pump, Sol. Energy 78 (2005) 331-339
12. M. Bojic, N. Nikolic, D. Nikolic, J. Skerlic, I. Miletic, Toward a positive-net-energy residential building in Serbian conditions, Appl. Energy 88 (2011) 2407-2419
13. J.A. Candanedo, A.K. Athienitis, Predictive control of radiant floor heating and solar-source heat pump operation in a solar house, HVAC R. Res 17 (3) (2011) 235-256

14. S. Li, J. Joe, J. Hu, P. Karava, System identification and model.predictive control of office building with integrated photovoltaic. thermal collectors, radiant floor heating and active thermal storage, Sol. Energy 113 (2015) 139-157

15. G.A. Dávi, E. Caamaño-Martín, R. Rüther, J. Solano, Energy performance evaluation of a net plus-energy residential building with grid-connected photovoltaic system in Brazil, Energy Build. 120 (2016) 19-29

16. A. Arteconi, E. Ciarrocchi, Q. Pan, F. Carducci, G. Comodi, Thermal energy storage with PV panels for demand side management of industrial building cooling loads, Appl. Energy 185 (2017) 1984-1993

17. A.K. de Wit, C.J. Wisse, Hydronic topologies for thermally activated building systems – design questions and case study, Energy Build. 52 (2012) 56-67

18. S.-H Cho, M. Zaherr-uddin, An experimental study of multiple parameter switching control for radiant floor heating systems, Energy 24 (1999) 433-444

19. M. Krzaczek, Z. Kowalczuk, Gain scheduling control applied to thermal barrier in systems of indirect passive heating and cooling of buildings, Control Eng. 20 (2012) 1325-1336

20. M. Gwerder, J. Tödli, B. Lehmann, V. Dorer, W. Güntensperger, F. Renggli, Control of thermally activated building systems (TABS) in intermittent operation with pulse width modulation, Appl. Energy 86 (2009) 1606-1616

21. M. Schmelas, T. Feldmann, E. Bollin, Adaptive predictive control of thermo-active building systems (TABS) based on a multiple regression algorithm, Energy Build. 103 (2015) 14-28

22. S. Prívara, J. Siroky, I. Ferkl, J. Cigler, Model predictive control of a building heating system: the first experience, Energy Build. 42 (2011) 564-572

23. B.W. Olesen, K. Sommer, B. Dïtching, Control of slab heating and cooling systems studied by dynamic computer simulations, ASHRAE Trans. 108 (2) (2000) 698-707

24. J. Romaní, G. Pérez, A. de Gracia, Experimental evaluation of a cooling radiant Wall coupled to a ground heat exchanger, Energy Build. 129 (2016) 484-490

25. J. Romaní, G. Pérez, A. de Gracia, Experimental evaluation of a heating radiant wall coupled to a ground source heat pump, Renew. Energy 105 (2017) 520-529

26. J. Romaní, L.F. Cabeza, A. de Gracia, Development and experimental validation of a transient “D numeric model for radiant walls, Submitted to Renew. Energy (June 2017)

27. EN ISO 6946 (2007), Building components and building elements – Thermal resistance and thermal transmittance – Calculation method

28. J.E. Seem, Modeling of heat transfer in Buildings, 1987, University of Wisconsin-Madison:Madison

29. G. Gebhart , Heat transfer, Second Edition, McGraw-Hill, (1971) 150-158

30. W.C. Swinback, Q.J. Roy, Long-wave radiation from clear skis, Q.J.R Meteorol, Soc.89 (1936) 339

31. S. Joan, D. Baggs, Australian earth-covered and green roof building 3rd ed. 2009: Dual Harmony publications

32. BITZER, https://www.bitzer.de (accessed June 2017)

33. ENDESA, https://www.endesaclientes.com/ (accessed June 2017)

34. M. Kottek, J. Grieser, C. Beck, B. Rudolf, F. Rubel, World map of Köppen-Geiger climate classification updated, Meteorol. Zeitschrift, 15 (2) (2006) 259-263

35. G.L. Barbose, N.R. Darghouth, Tracking the Sun IX: The installed price of residential and non-residential photovoltaic systems in the United States, CA. Lawrence Berkeley National Laboratory (2016)